Implementation options of a fully SiC Buck-CSI for advanced motor drive application

Yonghwa Lee and Alberto Castellazzi
Solid-State Power Processing (SP2) Lab
Kyoto University of Advanced Science
18, Gotanda-cho Yamanouchi, Ukyo Ward,
Kyoto, Japan, 615-8577
E-Mail: 2021md04@kuas.ac.jp

Keywords

«Current Source Inverter (CSI)», «Silicon Carbide (SiC)», «High-speed drive», «High frequency power converter», «High power density systems»

Abstract

This paper discusses the design option for a current source inverter for a 15kW high-speed machine with a wide-band-gap technology-based electric motor drive. Both control and modulation options are considered, as well as the integration of silicon carbide (SiC) bi-directional switches to yield high-performance bi-directional switches, as required by the topology. Recently, by taking advantage of the high-speed switching performance of SiC, a simple and robust control design method without voltage sensing and the Two-Third Modulation (TTM) method, which has the benefit of high efficiency, have been proposed. Based on this recent work, this paper proposes the simplified current-sensor-less controller of the CSI-fed PMSM. Also, this paper compared the characteristics of the TTM with the conventional PWM methods by simulation models.

Introduction

Research aiming at increasing efficiency and power density of power converters and machines is ubiquitous. A game-changing approach which has been receiving renewed and increasing attention in the very recent past is Current Source Inversion (CSI, or Current DC-Link Inversion). In this case, the square-wave PWM modulation of the output voltage followed by a filtering action is replaced by the direct synthesizing of a sinusoidal output voltage. In the pre-WBG era, application scenarios where CSIs could provide significant benefits were sparse and of limited relevance. Three-phase CSI topologies were mainly limited to boost (voltage step-up) and boost-buck (step-up step-down), but the proposed CSI concepts ended up mainly in obscurity or very niche applications. In comparison to VSI, the major benefits of CSI are:

- removal of dV/dt stress, eddy currents and common mode noise on the load;
- greatly improved harmonic signature, with virtual removal of any high-frequency harmonic components for greatly reduced motor losses;
- extremely high switching frequency capability for a given power rating, due to major reduction in the switching losses resulting from the twofold ability of employing lower-voltage-rated devices and switching them on average at lower peak voltages (decreasing sinusoidally to zero at the fundamental frequency);
- simpler circuit design and higher power densities.

So, the interest in CSI can be regarded as tightly related to the advent of WBG technology and, at present, the struggle for joint pursuit of increased efficiency and power density is renewing the momentum in CSI research [1-2]. Inherent advantageous features of CSI, Fig. 1 (a) such as joint inversion and voltage boosting capability, low output voltage harmonic distortion, removal of voltage DC-link and the related bulky capacitor technologies, are all very important for enabling disruptive progress beyond state-of-the-art in SiC-based power conversion, especially in the rapidly growing application domain of high-speed drives, as used increasingly in transportation.

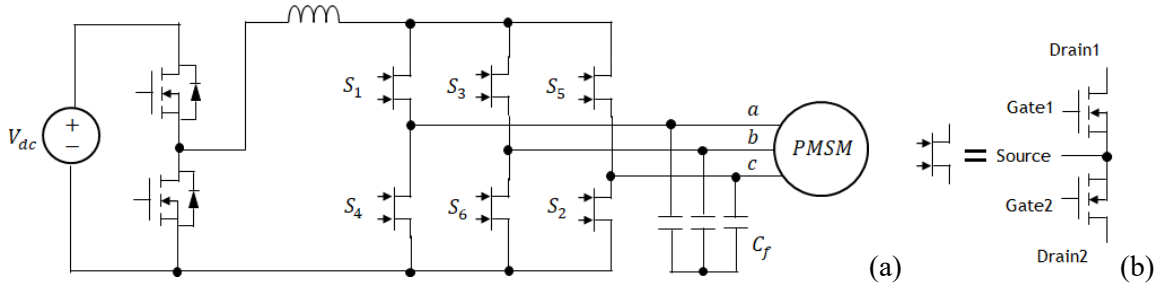

Fig. 1: Circuit schematic of Buck-CSI based motor-drive, with detail of bi-directional switch (BDS) implementation for the case of power MOSFETs (common source configuration).

Here, the aim is to go an important step further in enhancing efficiency and power density, with particular emphasis on future integrated electric drives: that will be pursued by original topology re-design and driving/control solutions and bespoke functional-structural integration. In particular, the converter requires a particular switch configuration: a bi-directional switch, capable of blocking voltage and conducting current in both directions (i.e., irrespective of the device terminals to the voltage and current are applied). The BDS schematic is shown in Fig. 1 (b); for the case of MOSFETs in common source configuration, by far the most practical implementation and favored solution. If built with discrete devices, the BDS cannot realistically be operated at the target high frequencies and thus enable disruptive progress in efficiency and power density: integrated SiC BDS`s are needed. Specifically, the BDS features a source-to-source connection between the two transistors. Whereas examples of monolithically integrated low-current GaN BDS`s have been shown, monolithic integration of SiC MOSFET is not viable, the difference being that GaN transistors are lateral devices, whereas SiC MOSFETs are vertical, with the source electrode corresponding to the semiconductor chip top surface. So, in view of the high integration aims of the project, design concepts and assembly solutions enabling the reliable top-to-top mounting of the devices are required, a world-first target in the framework of a technology development exercise targeting high-voltage large current capable industrial-grade solutions.

Pulse Width Modulation

In order to control gating signals for the switches of CSI, the space vector pulse width modulation (SVPWM) is developed [3]. The conventional SVPWM for VSIs are needed the dead time to avoid the arm short-circuit, which is the bottom, and the top switch turned on together at the same time. In contrast, the current source inverter requires overlap time during switching events when one device is being turned off while another is being turned on to ensure that a conducting path always exists for the dc-link inductor current to avoid the dangerous overvoltage from transient open circuits [4]. Therefore, the switching restraint for SVPWM of CSIs is that two switches should be conducted at any time of the current vectors.

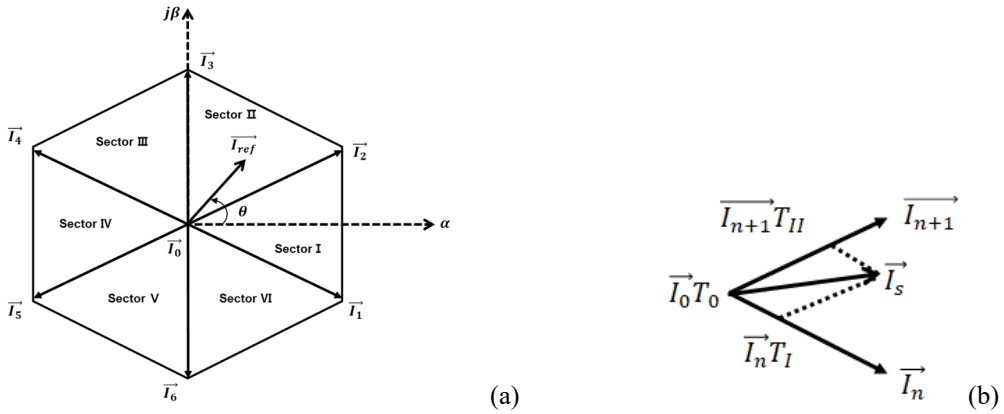

Fig. 2: Current Space Vector modulation.

As shown in Fig. 2(a), when operating CSI by SVPWM, the output current vector is divided into six sectors. A reference-current vector may be output by combining two active vectors and one zero vector for each vector, Fig. 2(b). Each active vector has a magnitude of a DC Link current, and if the DC-current may be controlled according to a target current, an optimized current vector may be output.

Table I: Switching state in CSIs and corresponding phase switching functions and switching space vectors

Three Zero Current Vectors					Six Active Current Vectors				
Vector	On Switches	$\vec{\iota_a}$	$\vec{\iota_b}$	$\vec{\iota_c}$	Vector	On Switches	$\vec{\iota_a}$	$\vec{\iota_b}$	$\vec{\iota_c}$
$\vec{I_0}$	S1, S4	0	0	0	$\vec{I_1}$	S6, S1	I_{dc}	$-I_{dc}$	0
$\vec{I_0}$	S2, S5	0	0	0	$\vec{I_2}$	S1, S2	I_{dc}	0	$-I_{dc}$
$\vec{I_0}$	S3, S6	0	0	0	$\vec{I_3}$	S2, S3	0	I_{dc}	$-I_{dc}$
					$\vec{I_4}$	S3, S4	$-I_{dc}$	I_{dc}	0
					$\vec{I_5}$	S4, S5	$-I_{dc}$	0	I_{dc}
					$\vec{I_6}$	S5, S6	0	$-I_{dc}$	I_{dc}

Looking at Table 1, CSIs have six active vectors and three zero vectors, and two switches must be operated in pairs to output them. The product of the current space vector and switching time is equated with the sum of the products of corresponding. The dwell time can be calculated with space vectors, and corresponding time intervals follow, where n is the number of the active vector. ($1 \le n \le 6$):

$$\vec{I_s}T_s = \vec{I_n}T_I + \overrightarrow{I_{n+1}}T_{II} + \vec{I_0}T_0 \quad (1)$$

$$T_s = T_I + T_{II} + T_0 \quad (2)$$

$$m_a = \frac{I_s^*}{I_{dc}}, \quad 0 \le m_a \le 1. \text{ where } I_s^* \text{is desired current} \quad (3)$$

$$T_I = m_a \sin\left(\frac{\pi}{6} - \left(\theta - \frac{(k-1)\pi}{3}\right)\right) T_s, \quad (4)$$

$$T_{II} = m_a \sin\left(\frac{\pi}{6} + \left(\theta - \frac{(k-1)\pi}{3}\right)\right) T_s \quad (5)$$

$$T_0 = T_s - T_I - T_{II} \quad k \text{ is the sector number. } (1 \le k \le 6) \quad (6)$$

In order to output the active vector and the zero vector, a sequence with a specific order must be created, as shown in Fig. 3. CSIs need to generate a specific switching sequence to implement SVPWM, and the losses and quality of output current may change according to the number and order of the sequences. Usually, five or seven sequences are used, but it can be seen that it is advantageous to have five switching sequences in terms of switching loss through the study [5].

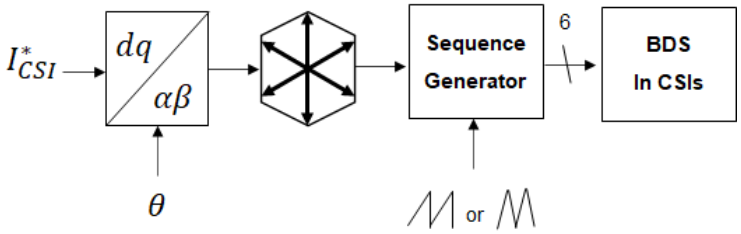

Fig.3: Space Vector PWM Generating Method of Current Source Inverters

Besides, according to a recent study [6], the six methods in Table 2 were discussed, and it can be seen that 8% of conduction loss and 86% of switching loss can be reduced when TTM is applied according to the modulation index. However, a DC-DC converter and synergetic control are required in this method.

Table 2: The state sequences

Modulation	State Sequence	Note
Asymmetric PWM	$[\overrightarrow{I_0}]\,[\overrightarrow{I_n}]\,[\overrightarrow{I_{n+1}}]$	CW-asymmetric pwm
	$[\overrightarrow{I_0}]\,[\overrightarrow{I_{n+1}}]\,[\overrightarrow{I_n}]$	CCW-asymmetric pwm
Symmetric PWM	$[\overrightarrow{I_n}]\,[\overrightarrow{I_0}]\,[\overrightarrow{I_{n+1}}]\,[\overrightarrow{I_0}]\,[\overrightarrow{I_n}]$	Zero Vector-symmetric pwm
	$[\overrightarrow{I_0}]\,[\overrightarrow{I_n}]\,[\overrightarrow{I_{n+1}}]\,[\overrightarrow{I_n}]\,[\overrightarrow{I_0}]$	In Vector-symmetric pwm
	$[\overrightarrow{I_0}]\,[\overrightarrow{I_{n+1}}]\,[\overrightarrow{I_n}]\,[\overrightarrow{I_{n+1}}]\,[\overrightarrow{I_0}]$	In+1 Vector-symmetric pwm
TTM	$[\overrightarrow{I_n}]\,[\overrightarrow{I_{n+1}}]$	without zero current vector

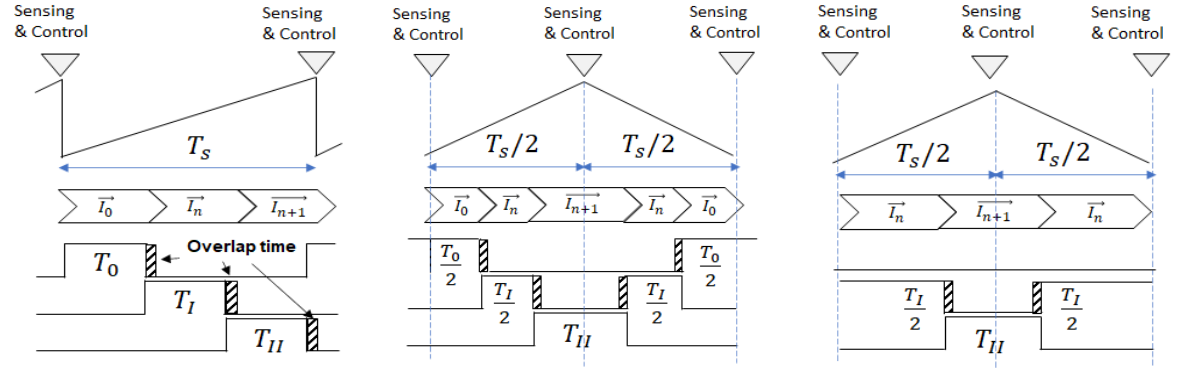

Asymmetric PWM (a) Symmetric PWM (b) Two-Third Modulation (c)

Fig. 4: (a) is shown that features of characteristic of Asymmetric PWM and (b) is indicated features of Symmetric PWM (c) is presented the characteristic of Two-Third Modulation.

As shown in the fig. 4, Symmetric PWM and TTM can be designed to facilitate the operation of sampling and control twice in one cycle period. In addition, since a switching operation of a power semi-conductor can affect the sensing precise for current and voltages, which is essential in respect of the control stability in practice, the asymmetric PWM must find a way to avoid the switching noise. Therefore, it may be considered that the symmetric PWM and TTM are more suitable for implementing a high-speed machine in practice.

In general, the CSI needs the power converter, which can control the dc-link current, since it prevents overcurrent and damage from the failure of switches. Thus, the dc-link current in the CSI can be controlled using the power converter to associate with the PWM method. Due to the existence of the zero current vector in the symmetric PWM, the limitation of the maximum modulation index should be considered when the dc-link current controls by the power converter. That is why the controlled dc-link current by the power converter must be higher than the desired output current of the CSI. However, in TTM, the controlled dc-link current can close to the desired output current of the CSI since the TTM only needs to generate the active current vector.

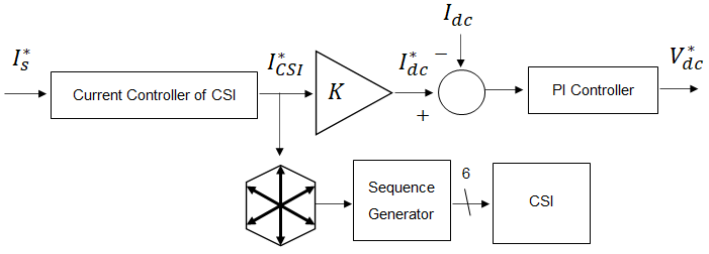

Fig. 5: The control concept for dc-link current controller; *K* is the margin for the limitation of pulse-width modulation method.

As a result of the simulation, Fig. 6 shows that the zero current vector was eliminated in the Two-Third Modulation compared to the conventional Symmetric PWM method. Additionally, due to the current of dc inductor ($i_{dc\ inductor}$) amplitude having a slight difference, the losses of using TTM might be decreased than the conventional PWM method.

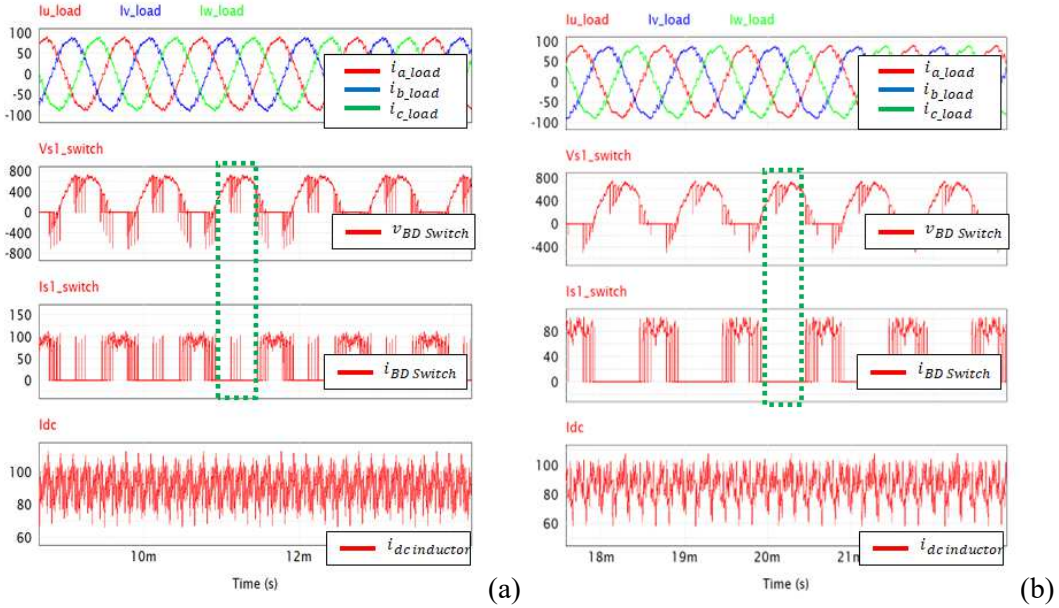

Fig. 6: The results of the simulation model (a) is shown that features of control characteristic of Symmetric PWM and (b) is indicated control features of Two-Third Modulation.

Design of the current controller for the CSI-fed PMSM

Due to their higher efficiency and power density, permanent magnet synchronous motors (PMSM) have replaced induction motors in many industrial applications, such as home applications and electric vehicles. That is why this paper proposes the control algorithm for the CSI-fed PMSM system.

The Current Source Inverter causes resonant frequency due to the Filter Capacitor connected to the output terminal. Previously, the Proportional and Resonant (PR) controller or the multi-nested-loop controller was proposed to control the LC resonant frequency. Since the system parameter error heavily influences these controllers, the complex vector controller and Active Damping Control Methods using the two-stage modeling of CSI-fed PMSM system have been studied to improve response performance in previous studies [7].

Recently, as high-speed switching became possible through the application of the Wide-Band-Gap switch, a method of simplifying and robust controller was proposed [8]. In particular, the multi-loop-nested controller required the voltage sensor of the filter capacitor and ac current sensors. However, it was possible to design a controller using only current sensors without additional voltage sensors in recent research [8].

On the other hand, the current sensor is generally more expensive than the voltage sensor and inhabits a slightly larger volume in the power electronics. In the case of Voltage Source Inverter, the method of reducing the number of current sensors using DC-Link current sensing has been widely proposed. Therefore, this paper proposes a design method that can simplify the controller using only the voltage sensor of the filter capacitor instead of the load-side ac current sensors.

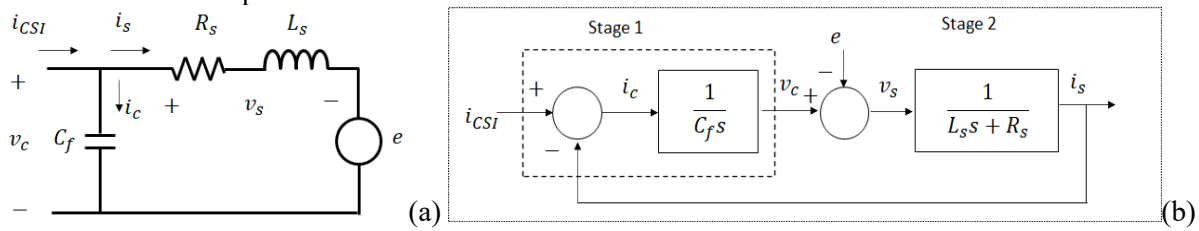

Fig. 7: (a) Equivalent circuit, and (b) Block diagram of CSI-fed PMSM in a stationary reference frame

First, for controller design, the system characteristics of the current source inverter with PMSM can be analyzed using two-stage modeling as in the previous study [7]. As illustrated in Fig, 7: *Cf* is the output filter capacitor, *e* is the machine electro-motive force, *Ls* the stator inductance, and *Rs* the stator resistance. Therefore, the plant of the system can represent by a second-order system (7).

$$G_p(s) = \frac{i_s(s)}{i_{CSI}(s)} = \frac{\frac{1}{L_s C_f}}{s^2 + s\frac{R_s}{L_s} + \frac{1}{L_s C_f}} \qquad (7)$$

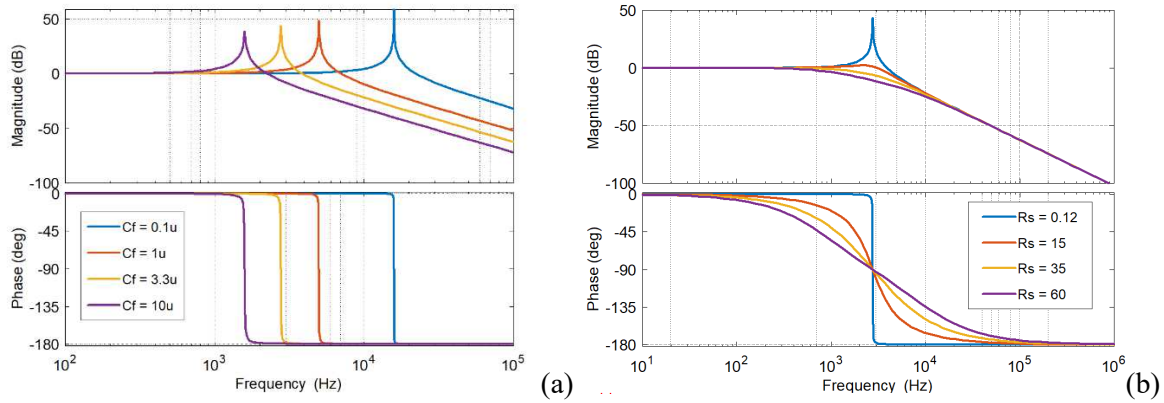

Fig. 8: The bode plot for the plant of current source inverter with PMSM, (a) depending on the output filter capacitance C_f, (b) depending on the stator resistance *Rs*.

Through the bode plot in Fig. 8, the resonance frequency can be adjusted according to the filter capacitance, and the resonance component can be controlled through the high-speed controller, so it is better to set it low enough compared to the switching frequency. Although, the gain and phase delay will be a problem if the resonant frequency is too low. In addition, if the stator resistance *Rs* can be increased, the resonance component can be damped, as shown in Fig. 8(b). By the way, in practice, increasing the resistance of the PM machine is not permitted because of the motor losses. Therefore, the controller could be designed to have the response characteristics of the desired 2nd-order system through the pole-zero cancellation technique as follows.

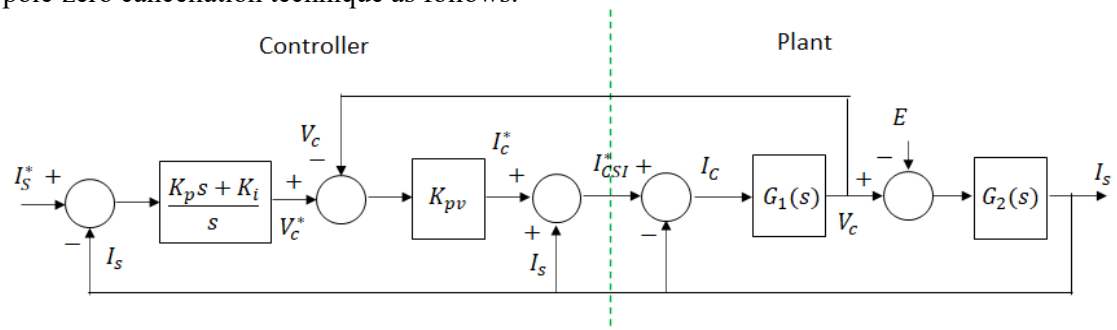

Fig. 9: The conventional multiple-nested-loop control design of CSI-fed PMSM

If the PI gain (K_p, K_i) are set as ($\widehat{L_s}\,\omega_{cc}, \widehat{R_s}\,\omega_{cc}$) respectively, and K_{pv} is $\widehat{C_f}\omega_f$, the transfer function can be induced as (10) where the estimated parameter(*hat*) are well matched.

$$G_1(s) = \frac{1}{sC_f} \qquad (8),$$

$$G_2(s) = \frac{1}{sL_s + R_s} \qquad (9)$$

$$CL(s) = \frac{I_s}{I_s^*} = \frac{\omega_f \omega_{cc}}{s^2 + \omega_f s + \omega_f \omega_{cc}} \qquad (10)$$

In recent research [8], a simple and robust voltage sensor-less controller was designed using the effect of the additional virtual resistance as follows in Fig. 10. C(s) is the proposed controller in the research [8].

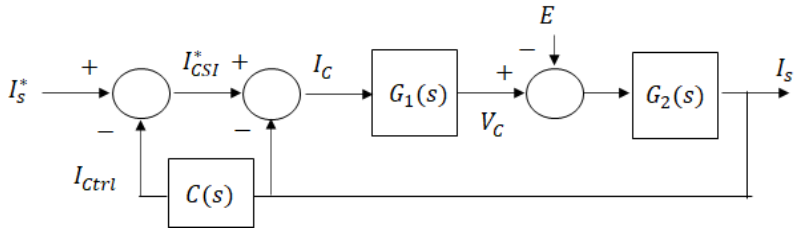

Fig. 10: The reference controller using only ac current sensor in the [8].

$$C(s) = \frac{I_{Ctrl}}{I_S} = sR_V\widehat{C_f} \qquad (11)$$

$$CL(s) = \frac{I_S(s)}{I_S^*(s)} = \frac{G_p(s)}{1 + G_p(s)C(s)} = \frac{\frac{1}{L_sC_f}}{s^2 + s\frac{(R_s + R_V)}{L_s} + \frac{1}{L_sC_f}} \qquad (12)$$

In order to obtain the fastest response corresponded to the critically damped system that contains no overshooting, the pole locations of the second-order system can be designed as:

$$Pole = -\frac{R_s}{2L_s} \pm \frac{1}{2}\sqrt{\frac{R_s^2}{L_s^2} - \frac{4}{L_sC_f}} \qquad (13)$$

$$\frac{R_s^{*2}}{L_s^2} - \frac{4}{L_sC_f} = 0\,, \quad R_s^* = 2\sqrt{\frac{L_s}{C_f}} \cong 35.0\,\Omega \qquad (14)$$

$$R_v = R_s^* - R_s = 34.88\,\Omega \qquad (15)$$

As mentioned above, the use of voltage sensors may have advantages over the use of current sensors in the aspect of price and volume. Therefore, in this paper, the controller with the same response characteristics as discussed above [8] can be designed as follows.

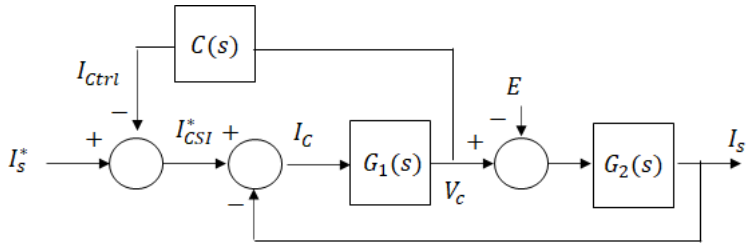

Fig. 11: The block diagram of proposed controller and system which has only voltage sensors.

$$C(s) = \frac{I_{Ctrl}}{V_C} = \frac{sR_V\widehat{C_f}}{s\widehat{L_s} + \widehat{R_S}}, \qquad (16)$$

$$CL(s) = \frac{I_S(s)}{I_S^*(s)} = \frac{\frac{G_1(s)\,G_2(s)}{1 + G_1(s)\,C(s)}}{1 + \frac{G_1(s)G_2(s)}{1 + G_1(s)\,C(s)}} = \frac{\frac{1}{L_sC_f}}{s^2 + s\frac{(R_s + R_V)}{L_s} + \frac{1}{L_sC_f}} \qquad (17)$$

There is a difference between the previous study [8] and the proposed controller. Since the reference controller has the derivative, the filtered discrete derivative is considered when expanding in the discrete-time domain because the filter can reduce the emitting disturbance, such as sensing noise. In contrast, the proposed controller in this paper basically has a feature like the High Pass Filter. However,

due to the nature of the High Pass Filter, it may have the DC offset problem, so consideration of this should be sufficiently studied when expanding the controller in the discrete-time domain.

Table 3: The parameters of the simulation model

Parameters	**Value**	**Parameters**	**Value**
CSI output power	15kW	Rotor Type	SPM
Pole / Slots	12 / 18	Motor Phase inductance	1.0 mH
Input DC Voltage	500 Vdc	Motor Phase resistance	0.12 Ω
DC link Inductance	600uH	Switching Frequency in CSI	75kHz
Switching Frequency in DC-DC Converter	75kHz	Filter capacitor	3.3uF
Overlap Time	200ns	Fundamental frequency	540Hz (electrical)

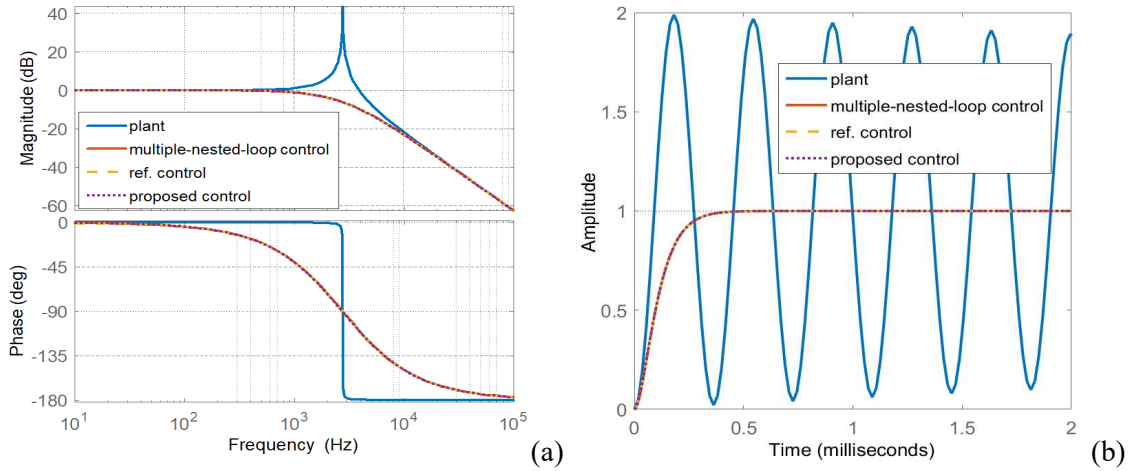

Fig. 12: (a) Bode plot and (b) unit step response for comparison the characteristic of system response depending on the plant with open-loop and the controller which are mentioned this paper.

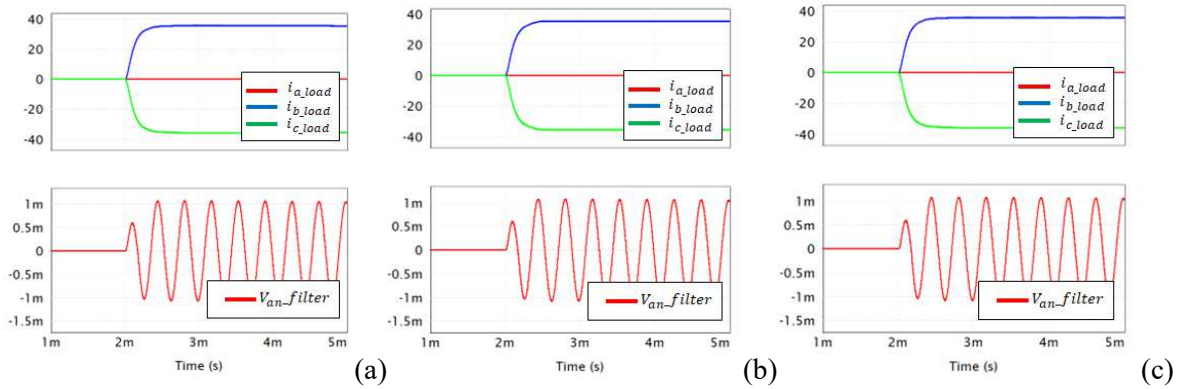

Fig. 13: Step Response depending on the controller design; (a) Conventional multiple-nested-loop controller, (b) Reference controller without voltage sensors, (c) Proposed controller without ac current sensors.

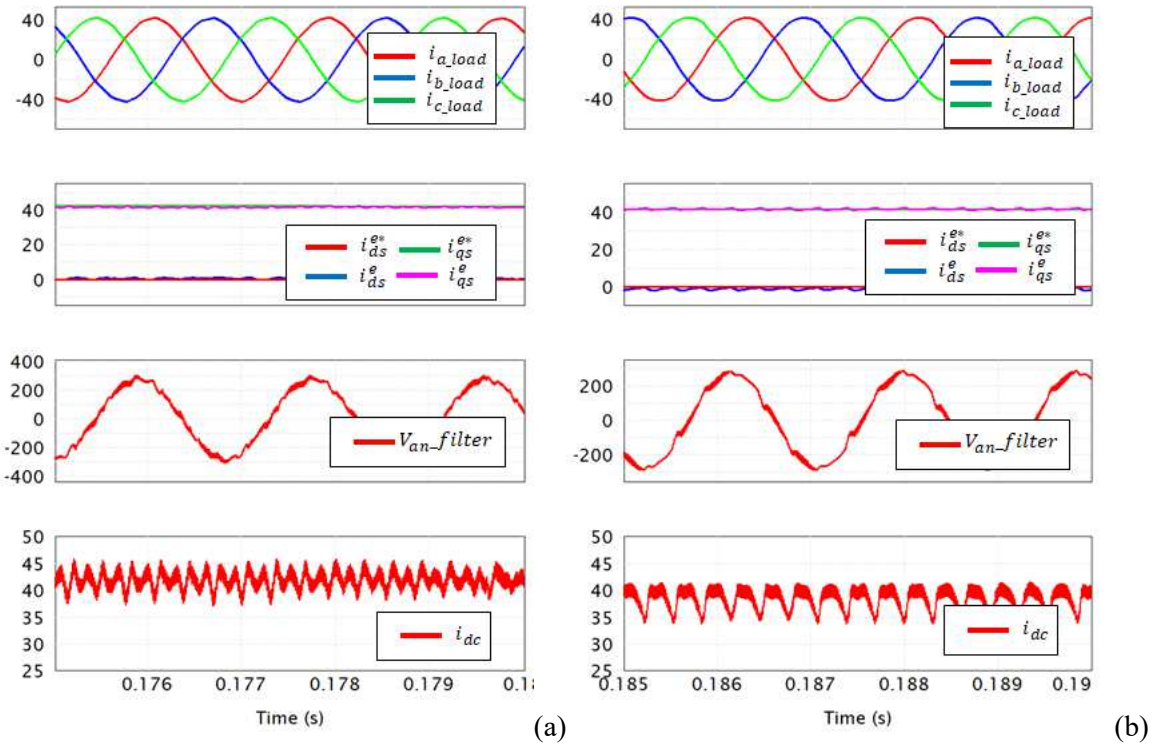

Fig. 14: Simulation Result of the proposed controller under the different PWM strategy between Symmetric PWM (a) and Two-Third PWM (b).

As can be seen from the bode plot in Fig. 12, it has almost the same response characteristics in continuous time domain. However, as seen in the recent paper [8], due to the derivative component, it can be a problem in stability, such as the disturbance. Therefore, further design is needed to allow the control design in the discrete time domain to have robust properties against possible disturbances such as harmonic components of EMF and sensing noise. This can be discussed through future research.

As shown in Fig. 13, the simulation results of 40A step responses below verified that each controller has similar response characteristics through RL load. The simulation result for the step response was performed by applying Symmetric PWM, and it was intended to verify the response characteristics of the current controller through DC Aline current. It can be said that the current controller designed through this has basically similar performance. However, as mentioned earlier, the impact on the error of the motor parameter and disturbance will be verified through further research.

In Fig 14, it could be verified through the simulation model that the proposed controller can be stably controlled at 15 kW load conditions by applying it under Symmetric PWM and Two-Third PWM to CSI-fed PMSM. Also, this result shows the control of the DC-DC converter varies depending on the Symmetric PWM and TTM methods. Although it has the same inverter output power current under the same load conditions, for TTM, it is essential to control the DC Link current in order to remove the Zero Current Vector. The harmonic of the current also increases depending on the shape of the DC current, so attention should be paid to the DC current control. On the other hand, in the case of Symmetric PWM, the DC Link current should be controlled in the DC constant with the Modulation Margin required by CSI so that the higher current should be controlled compared to the TTM. Accordingly, the losses of the power converter may be additionally generated compared to the TTM. However, since the harmonics of the output current control the DC current in a DC form, it may be said to be less than that of TTM. In other words, as shown in the previous study [6], in the case of TTM, attention to the syngeneic control between CSI and DC converter is required.

Finally, the simplified controller can reduce the mass on computational processors (e.g., microprocessor) because it has less computation and less input from sensors than the conventional controller [7,8]. That is, the high-speed controller operation through the high-speed switching power semiconductor may cause a cost increase mass of the control processor. However, the computational mass may be reduced using the simplified controller. It will be able to suppress the mass on the processor.

HW Development

Finally, for the hardware implementation, the creation of custom integrated high electro-magnetic and electro-thermal performance SiC MOSFET BDS`s is proposed, taking the moves from a concept developed and already successfully demonstrated for the case of a matrix converter [9, 10]. Here, Fig 15, the proposed concept of SiC MOSFET BDS differs from the previous one proposed for the Matrix Converter by horizontally connecting common sources to increase the heat dissipation area for application to Integrated Motor Drives with high temperatures and poor environmental conditions. The innovative packaging concept relies on a Power Overlay (POL) concept, capable of withstanding high temperatures, in excess of 200 °C [11]. In the future, the design will be verified through further research such as thermal analysis and experiments.

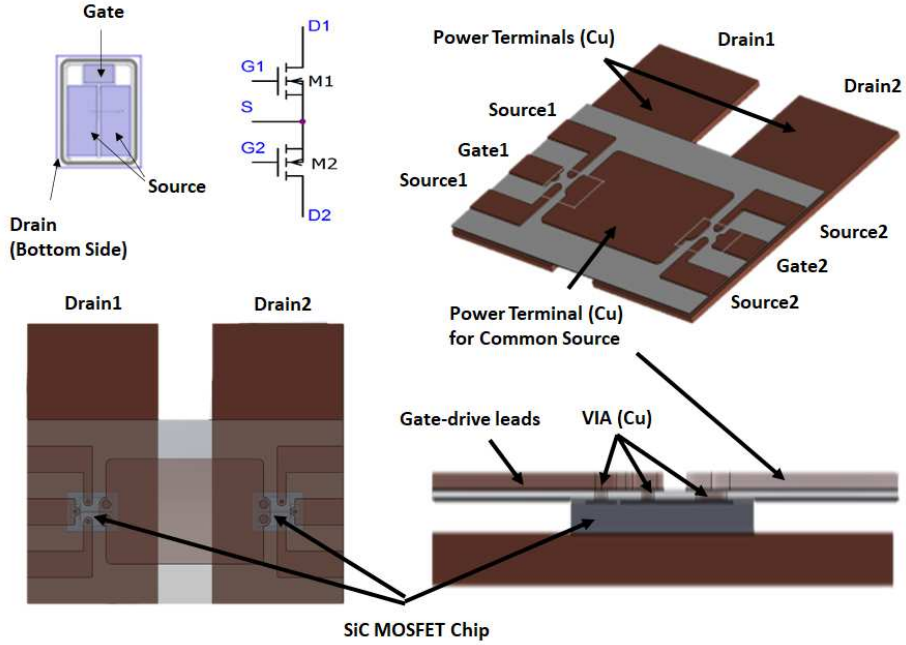

Fig. 15: The proposed design concept of the SiC Bi-directional Switch Power Module

Conclusion and Future work

Several pieces of research have recently been studied on the Current Source Inverter by taking advantage of the high switching frequency enabled by WBG devices. In this paper, the method to effectively control and implement these powerful functions has been discussed.

This research discussed the modulation technique and the design of the simplified current controller with respect to the new technologies of the current source inverter using the wide-band-gap power semiconductor, which is actively researched and proposes a new current controller to reduce the current sensors. Furthermore, we assess the PWM of CSI through Simulation Model and verify the proposed controllers.

Based on this study, we will continue to study various problems of the proposed controller through discrete-time analysis, i.e., current offset errors and so on. Accordingly, it is intended to extend from CSI to rotor position estimation technology using minimal sensors, such as Voltage Source Inverter, which can follow the rotor position of PMSM using only DC-Link voltage and current measurement. In addition, to develop future Integrated Motor Drives, we intend to verify and evaluate the Power Module design of SiC-based Bi-direction Switches suitable for CSI.

References

[1] J. W. Kolar and J. Huber, "Next-Generation SiC/GaN Three-Phase Variable-Speed Drive Inverter Concepts," PCIM Europe digital days 2021; International Exhibition and Conference for Power Electronics, Intelligent Motion, Renewable Energy and Energy Management, 2021, pp. 1-5.

[2] R. Amorim Torres, H. Dai, W. Lee, B. Sarlioglu and T. Jahns, "Current-Source Inverter Integrated Motor Drives Using Dual-Gate Four-Quadrant Wide-Bandgap Power Switches," in IEEE Transactions on Industry Applications, vol. 57, no. 5, pp. 5183-5198, Sept.-Oct. 2021, doi: 10.1109/TIA.2021.3096179.

[3] Y. W. Li, B. Wu, D. Xu and N. R. Zargari, "Space vector sequence investigation and synchronization methods for active front-end rectifiers in high-power current-source drives," IEEE Trans, Industrial Electronics, vol. 55, no. 3, pp. 1022-1034, Mar. 2008

[4] R. A. Torres, H. Dai, W. Lee, T. M. Jahns and B. Sarlioglu, "Current-Source Inverters for Integrated Motor Drives using Wide-Bandgap Power Switches," 2018 IEEE Transportation Electrification Conference and Expo (ITEC), 2018, pp. 1002-1008, doi: 10.1109/ITEC.2018.8450127.

[5] M. G. Sayed, O. Abdel-Rahim and M. Orabi, "Comparative Study to Investigate the Effect of Five VS Seven Segment Modulation Sequence on the Waveform Distortion Resulted by the Overlap Time in Current Source Inverter," 2019 International Conference on Innovative Trends in Computer Engineering (ITCE), 2019, pp. 576-580, doi: 10.1109/ITCE.2019.8646346.

[6] M. Guacci, M. Tatic, D. Bortis, J. W. Kolar, Y. Kinoshita and H. Ishida, "Novel Three-Phase Two-Third-Modulated Buck-Boost Current Source Inverter System Employing Dual-Gate Monolithic Bidirectional GaN e-FETs," 2019 IEEE 10th International Symposium on Power Electronics for Distributed Generation Systems (PEDG), 2019, pp. 674-683, doi: 10.1109/PEDG.2019.8807580.

[7] H. Lee, S. Jung and S. Sul, "A current controller design for current source inverter-fed PMSM drive system," 8th International Conference on Power Electronics - ECCE Asia, 2011, pp. 1364-1370, doi: 10.1109/ICPE.2011.5944414.

[8] R. A. Torres, H. Dai, W. Lee, T. M. Jahns and B. Sarlioglu, "A Simple and Robust Controller Design for High-Frequency WBG-Based Current-Source-Inverter-Fed.AC Motor Drive," 2020 IEEE Transportation Electrification Conference & Expo (ITEC), 2020, pp. 111-117.

[9] Aliyu, A. M., Castellazzi, A., Lasserre, P., & Delmonte, N. (2017, June). Modular integrated SiC MOSFET matrix converter. In 2017 IEEE 3rd International Future Energy Electronics Conference and ECCE Asia (IFEEC 2017-ECCE Asia) (pp. 1184-1188). IEEE.

[10] P. Lasserre, D. Lambert and A. Castellazzi, "Integrated Bi-directional SiC MOSFET power switches for efficient, power dense and reliable matrix converter assembly," 2016 IEEE 4th Workshop on Wide Bandgap Power Devices and Applications (WiPDA), 2016, pp. 188-193.

[11] https://www.shinko.co.jp/english/product/package/assembly/pol.php